Thermal Behaviors and Optical Parametric Oscillation in 4H-Silicon Carbide Integrated Platforms

Shi, Xiaodong; Fan, Weichen; Hansen, Anders Kragh; Chi, Mingjun; Yi, Ailun; Ou, Xin; Rottwitt, Karsten; Ou, Haiyan

Published in:
Advanced Photonics Research

Link to article, DOI:
10.1002/adpr.202100068

Publication date:
2021

Document Version
Publisher's PDF, also known as Version of record

ADVANCED PHOTONICS RESEARCH
www.adpr-journal.com

Thermal Behaviors and Optical Parametric Oscillation in 4H-Silicon Carbide Integrated Platforms

*Xiaodong Shi, Weichen Fan, Anders Kragh Hansen, Mingjun Chi, Ailun Yi, Xin Ou, Karsten Rottwitt, and Haiyan Ou**

4H-silicon carbide (SiC) integrated platforms have shown great potential in quantum and nonlinear photonics. However, the thermal properties of 4H-SiC waveguides are still unknown, even though thermo-optic effects can play an important role in fundamental measurements and practical applications. Herein, the thermo-optic effects in a 4H-SiC microring resonator are comprehensively studied, by means of both temperature tuning and self-heating. The thermo-optic coefficient and the ratio between the thermal absorption and the thermal diffusion of 4H-SiC are quantitatively measured to be $4.21 \times 10^{-5}\,\mathrm{K}^{-1}$ and $14.9\,\mathrm{K\,W}^{-1}$, respectively. Considering the acquired thermal properties, Kerr-nonlinearity-based dual-pump optical parametric oscillation (OPO) is experimentally achieved, and thus, it is demonstrated that broadband solitons can feasibly be generated through thermal tuning of 4H-SiC-on-insulator (SiCOI) microring resonators.

1. Introduction

Integrated photonics enable on-chip quantum and classical signal processing for optical communication with compact optical devices and systems.[1,2] Silicon is one of the most widely used materials for integrated photonics, but suffers from strong two-photon absorption and free-carrier absorption, making the material poorly suited for high-power nonlinear applications.[3] These shortcomings result in an increasing presence of different integrated platforms with wide bandgap optical materials, such as Si_3N_4, AlN, $LiNbO_3$, and silicon carbide (SiC).[4–7] SiC is a mature material that has been widely used in the power electronic and mechanic fields, due to its high breakdown field ($3 \times 10^{-6}\,\mathrm{V\,cm}^{-1}$), large Young's modulus (450 GPa), and high chemical inertness.[8,9] In the past decade, SiC has started to become increasingly used for integrated photonics because of the additionally beneficial optical properties of low intrinsic propagation loss ($0.3\,\mathrm{dB\,cm}^{-1}$), large refractive index (2.6 at 1.55 μm), and a broad transparent window from the near UV to the mid-IR wavelength range. A variety of nano- and microcavities with strong light enhancement, including microrings, microdisks, and photonic crystals, have been experimentally demonstrated in 3C, 4H, 6H, and amorphous SiC (a-SiC) integrated platforms.[7,10–21] Compared with the other polytypes of SiC, 4H-SiC exhibits both diverse promising color centers and high second- and third-order nonlinearities and is, thus, more interesting within quantum and nonlinear photonics.[7,12,22]

Thermal properties play an important role in light propagation in optical media. Thermal impact on optical devices can be caused either by changes in the surrounding temperature or by self-heating due to light absorption in the material, and often leads to mode instabilities. Light absorption can dramatically heat the devices, especially in microring resonators, because the optical power is significantly enhanced inside the cavity. Even a slight thermally induced microring resonance drift may cause wavelength detuning or phase mismatch, degrade the nonlinear processes, and completely change the device behavior.[23] However, thermal effects can also, sometimes, be exploited. The resonance shift of microring resonators has been applied for making tunable band-pass and band-elimination filters, modulators, and multiplexers.[24,25] Thermal tuning is also a crucial approach to generate frequency combs, to adjust the frequency line spacing, and to control the mode locking of the solitons in microring resonators.[26,27] Moreover, thermally induced optical bistability holds great potential for all-optical classical and nonclassical signal processing.[28–30] Therefore, the thermal properties of 4H-SiC integrated platforms are highly important to explore, for the purpose of achieving more advanced experimental results and applications with better performance.

Kerr-nonlinearity-based optical parametric oscillation (OPO), resulting from cascaded four-wave mixing (FWM), is a promising candidate for monolithic tunable light sources[31] and is also regarded as an important precondition of integrated frequency

X. Shi, W. Fan, Dr. A. K. Hansen, Dr. M. Chi, Prof. K. Rottwitt, Dr. H. Ou
DTU Fotonik
Technical University of Denmark
Lyngby DK-2800, Denmark
E-mail: haou@fotonik.dtu.dk

A. Yi, Prof. X. Ou
State Key Laboratory of Functional Materials for Informatics
Shanghai Institute of Microsystem and Information Technology
Chinese Academy of Sciences
Shanghai 200050, China

The ORCID identification number(s) for the author(s) of this article can be found under https://doi.org/10.1002/adpr.202100068.

DOI: 10.1002/adpr.202100068

comb (microcomb) generation.[32] OPO in microresonators with a single pump exhibits a certain threshold power, which is determined by the quality factor of the resonator,[33] whereas a dual-pump scheme can trigger OPO through nondegenerated FWM and theoretically is thresholdless, alleviating the demand on high pump power.[34] Microcavity solitons, as mode-locked microcombs, are favorable in practical applications because of their stability and robustness.[35] In recent years, tremendous efforts have been made to generate microcavity solitons, and several methods have been successfully demonstrated, including pump frequency scanning, power kicking, as well as self-injection locking.[36–38] Thermal tuning provides another strategy that can use fixed lasers with narrower linewidth as the pumps instead of tunable ones, and, thus, reduce the noise and spectral linewidth of solitons.[27]

In this work, we comprehensively study the temperature-dependent effective index and group index, and find the relation between the incident power and the temperature change through self-heating in 4H-SiC microring resonators. Dual-pump OPO is achieved by the pump sweeping scheme, and the potential for soliton formation using thermal tuning is proposed. Our results demonstrate the possibility of broadband OPO and soliton generation in 4H-SiC-on-insulator (SiCOI) microresonators and are meaningful for either improving the thermal stability or taking advantages of thermo-optic effects in the 4H-SiCOI integrated platforms.

2. Thermal Properties of 4H-SiC Microring Resonators

To measure the thermal effects, we fabricated a microring resonator in the 4H-SiCOI integrated platform, with a radius R of 33 μm and a cross section of 1200 nm × 400 nm, as shown in **Figure 1**a. The linear transmission of the transverse electric (TE) polarized mode in the microring resonator is plotted in Figure 1b. Both TE_{00} and TE_{10} modes emerge in the spectrum. They can be distinguished by the difference in the free spectral range (FSR), f_{FSR}. As the group index, n_g, of the TE_{00} mode is smaller than that of the TE_{10} mode, the FSR of the TE_{00} resonance, equal to 482 GHz, is larger than that of the TE_{10} resonance, equal to 460 GHz. The following study is based on the TE_{00} resonance, as shown in Figure 1c, which has a full-width at half-maximum (FWHM) of $\Delta\lambda_{FWHM} = 33$ pm and a quality factor of $Q = \frac{\lambda}{\Delta\lambda_{FWHM}} = 4.7 \times 10^4$ at $\lambda = 1548.1$ nm. The microring resonantor operates in the undercoupled regime, so the intrinsic and external quality factors can be calculated by $Q_{in} = \frac{2Q}{1+\sqrt{\Gamma}} = 6.1 \times 10^4$ and $Q_{ex} = \frac{2Q}{1-\sqrt{\Gamma}} = 20 \times 10^4$, respectively, where Γ is the extinction ratio of the transmittance. The propagation loss is estimated through $\alpha = \frac{2\pi n_g}{Q_{in}\lambda} = 8.6\,\mathrm{dB\,cm^{-1}}$.[39]

2.1. Temperature-Dependent Thermal Properties

The resonance wavelength of the microring resonator follows[40]

$$m\lambda = n_{eff} \times 2\pi R \tag{1}$$

where m is an integer, and n_{eff} is the effective refractive index of the resonant mode. Thermal effects can influence the resonance by altering both the refractive index and the geometric structure;[41] thereby, the variation of resonance versus temperature T is given by

$$m\frac{d\lambda}{dT} = 2\pi R\frac{dn_{eff}}{dT} + 2\pi n_{eff}\frac{dR}{dT} \tag{2}$$

Substituting Equation (1) into (2), one obtains

$$\frac{1}{\lambda}\frac{d\lambda}{dT} = \frac{1}{n_{eff}}\frac{dn_{eff}}{dT} + \frac{1}{R}\frac{dR}{dT} \tag{3}$$

wherein the thermo-optic coefficient, dn_{eff}/dT, is the rate of change of the refractive index with temperature, and $a = \frac{1}{R}\frac{dR}{dT}$ is the relative thermal expansion along the radial direction. It is seen that a positive thermo-optic coefficient along with thermal expansion results in a red shift of the resonance, as the temperature increases. As the microring resonator is fabricated on 4H-SiC with the c-axis parallel to [0001] crystal orientation, the thermal expansion of the radius can be obtained by[42]

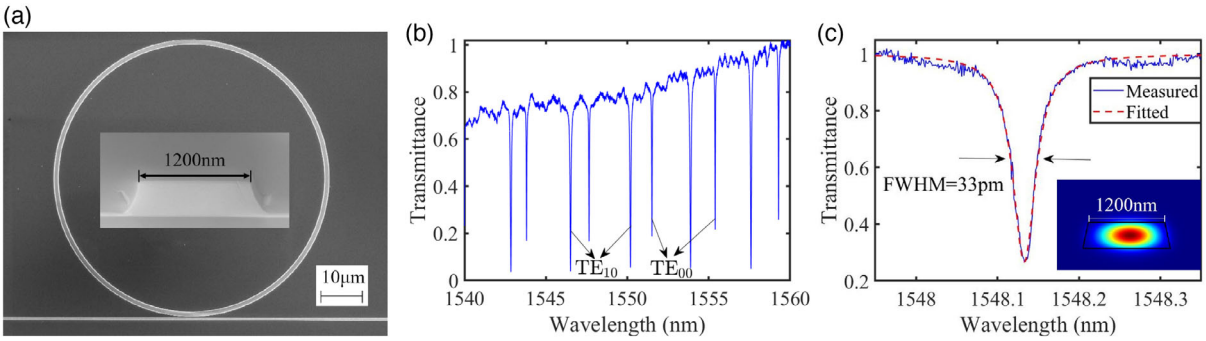

Figure 1. 4H-SiC microring resonator characterization. a) Scanning electron microscopy image of the device top view. The inset shows the cross section of the microring. b) Normalized transmission spectrum measured at 297.6 K with an input power of 10 μW. Both TE_{00} and TE_{10} resonances can be observed. c) Normalized measured (blue) and fitted (red) spectrum of TE_{00} resonance at 1548.1 nm, with an FWHM of 33 pm, at 297.6 K with an input power of 10 μW. The inset shows the simulated TE_{00} mode profile.

$$a = 3.21 \times 10^{-6} + 3.56 \times 10^{-9}(T - 273.15) - 1.62 \times 10^{-12}(T - 273.15)^2 \mathrm{K}^{-1} \quad (4)$$

The thermal effects are measured by placing the photonic chip on top of a plate, that is, temperature controlled and monitored by a thermoelectric cooler (TEC). The resonance shift as a function of the temperature, with respect to a reference temperature of 297.6 K, is plotted in **Figure 2**a in blue. In the investigated temperature range from 284 to 339 K, the resonance shift is found to be linear with temperature, with a fitted slope of $\frac{d\lambda}{dT} = 0.0344 \pm 0.0003\,\mathrm{nm\,K^{-1}}$. It is found from Equation (4) that the thermal expansion is on the order of $10^{-6}\,\mathrm{K}^{-1}$ at room temperature, which is usually considered to be negligible in materials with large $\frac{dn_{\mathrm{eff}}}{dT}$, such as silicon and AlGaAs. However, we find that the thermal expansion obviously contributes to the resonance shift of the SiC microring resonator, as shown in Figure 2a in red, wherein the two cases, with and without considering the thermal expansion, are analyzed. Without thermal expansion, the thermo-optic coefficient is calculated and fitted to be $\frac{dn_{\mathrm{eff}}}{dT} = 4.94 \times 10^{-5}\,\mathrm{K}^{-1}$, whereas with the thermal expansion, it becomes $\frac{dn_{\mathrm{eff}}}{dT} = 4.21 \times 10^{-5}\,\mathrm{K}^{-1}$. It indicates that the thermal expansion can induce 17% difference on the thermo-optic coefficient; as a result, it is a nonnegligible thermal effect. It is noticed that the microring resonator is made of a SiC core, embedded in SiO_2 surroundings. As the majority of the light is confined in the SiC core, shown in the inset of Figure 1c, and the thermo-optic coefficient of SiO_2 is below $0.6 \times 10^{-5}\,\mathrm{K}^{-1}$,[41] much lower than that of 4H-SiC; thus, we are convinced that the influence of SiO_2 can be neglected, and the measured thermo-optic coefficient is dominated by the 4H-SiC core.

Compared with other SiC integrated platforms listed in **Table 1**, 4H-SiC has the largest thermo-optic coefficient among all the crystalline SiC, but it is lower than that of the a-SiC. Such large thermo-optic coefficient indicates that 4H-SiC allows for efficient tuning of the optical devices using, for example, microheaters, but, at the same time, indicates a sensitivity to environmental perturbations and absorption-induced thermal instability, potentially posing an issue for some critical nonlinear processes.

Table 1. Thermal-optic coefficient of different SiC integrated platforms.

Platform	$\frac{dn_{\mathrm{eff}}}{dT}$ [K^{-1}]	Consider thermal expansion
3C-SiCOI[13]	2.67×10^{-5} @295.4 K	No
6H-SiCOI[48]	3.87×10^{-5} @298.2 K	No
a-SiCOI[14]	1.4×10^{-4} @298.1 K	Yes
4H-SiCOI (this work)	4.21×10^{-5} @297.6 K	Yes

Furthermore, as different wavelength has different response to thermal effects, the FSR and the group index can also be affected, which is derived as

$$-\frac{1}{f_{\mathrm{FSR}}}\frac{df_{\mathrm{FSR}}}{dT} = \frac{1}{n_g}\frac{dn_g}{dT} + a \quad (5)$$

This indicates that the FSR decreases with increasing group index, as well as with thermal expansion. In the experiment, the adjacent resonances on both sides of the investigated resonance are measured for obtaining the FSR. Figure 2b shows the FSR variation as a function of the temperature in blue. In general, the FSR decreases linearly with the increasing temperature, with a slope based on the fit of $\frac{f_{\mathrm{FSR}}}{dT} = -0.011 \pm 0.002\,\mathrm{GHz\,K^{-1}}$. The corresponding group index change as a function of the temperature, considering the thermal expansion effect, is plotted in Figure 2b in red. The group index increases linearly, as the temperature increases, with a slope of $\frac{dn_g}{dT} = 5.7 \times 10^{-5}\,\mathrm{K}^{-1}$. The difference of the temperature dependence between the group index and the effective index shows that the temperature is also able to change the waveguide dispersion.

2.2. Absorption-Induced Thermal Properties

Besides the external temperature variation, the input power of the incident light can also change the temperature of the microring resonator, as a result of the thermal absorption and diffusion, which obeys[43]

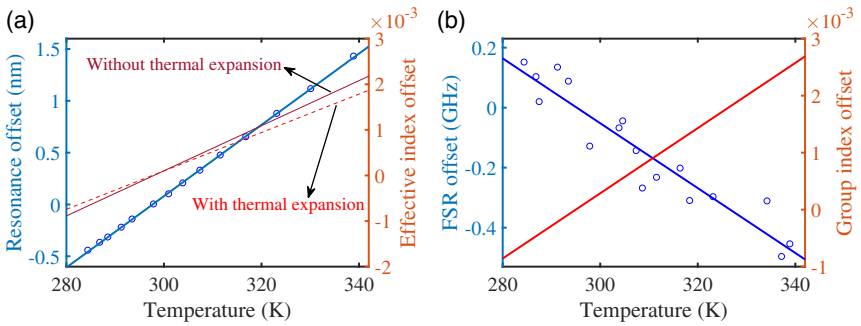

Figure 2. a) Measured (blue circles) and fitted (blue line) resonance offset (left axis) of the microring resonator, and the corresponding effective index offset (right axis), calculated without (red solid line) and with (red dash line) the consideration of the thermal expansion, with respect to the temperature. b) Measured (blue circles) and fitted (blue line) FSR offset (left axis) of the microring resonator, and the corresponding group index offset (right axis), calculated with the consideration of the thermal expansion, with respect to the temperature.

$$\frac{d\Delta T}{dt} = -\eta_{diff}\Delta T + \eta_{abs} P_{intra} \tag{6}$$

where t is the time, and η_{diff} and η_{abs} denote the thermal diffusion and the absorption rate, respectively. P_{intra} is the intracavity power that can be calculated from the on-chip input power in the bus waveguide, P_{input}, and the field enhancement factor, F[44]

$$P_{intra} = F^2 P_{input} \tag{7}$$

$$F^2 = \frac{\kappa}{1 - 2\sqrt{(1-\kappa)\exp(-\alpha L)}\cos(\frac{2\pi}{\lambda}L) + (1-\kappa)\exp(-\alpha L)} \tag{8}$$

where κ denotes the coupling coefficient that is 0.0125 for our microring resonator, and L is the circumference of the microring resonator. If the light is resonant, the field enhancement factor can be simplified to

$$F^2 = \frac{\kappa}{1 - 2\sqrt{(1-\kappa)\exp(-\alpha L)} + (1-\kappa)\exp(-\alpha L)} \tag{9}$$

When the light couples from the bus waveguide into the investigated microring resonator, the power is significantly enhanced by a factor of 17.7, based on Equation (9).

Figure 3 (left-bottom axis) shows the resonance shift as a function of the input power. The resonance shift increases linearly with the input power, with a fitted slope of $\frac{d\lambda}{dP_{input}} = 8.7 \pm 0.3\,\mathrm{nm\,W^{-1}}$. The change of the effective index can be jointly contributed by the Kerr effect and the thermo-optic effect because of the high field strength and the self-heating from the material absorption of the light inside the microring resonator, respectively. The Kerr effect-induced refractive index change is proportional to the intensity of the light in the medium, given by $\Delta n = n_2 I$, where n_2 is the nonlinear refractive index. Using $n_2 = 6 \times 10^{-19}\,\mathrm{m^2\,W^{-1}}$ of 4H-SiC,[10] we find that the contribution to the refractive index change from the Kerr effect is three orders of magnitude smaller than that of the thermo-optic effect. Thus, the resonance shift is dominated by the thermo-optic effect. Combining the relationship of resonance shift versus temperature and resonance shift versus input power, the temperature can one-to-one map the intracavity power, as shown in Figure 3 (right-top axis). The temperature increases linearly with the intracavity power, with a slope of $\frac{dT}{dP_{intra}} = 14.9\,\mathrm{K\,W^{-1}}$, which is also the ratio between the thermal absorption rate and the thermal diffusion rate according to Equation (6) for the stable state.

2.3. Optical Bistability

We also observe optical bistability in the 4H-SiC microring resonator, which is shown in **Figure 4**. A tunable laser source is used to sweep the resonance at room temperature, showing a transmittance that is not only power-dependent, but also depends on the sweeping direction. The optical bistability starts to become apparent at an input power of about 12 mW, and it becomes stronger with higher input power. When sweeping the resonance from short to long wavelength, the light is coupled into the resonator and heats up the microring resonator. As the intracavity power increases, the thermo-optic effect is enhanced and pushes the resonance toward longer wavelength. The sweeping wavelength is chasing the resonance wavelength, as the detuning decreases. Upon reaching the on-resonance circumstance, that is the sweeping wavelength exactly matches the resonant wavelength and the power coupled into the resonator is maximal, the resonance reaches the largest shift. With the on-going sweeping toward longer wavelength, the power coupled into the ring decreases, resulting in a blue shift of the resonance. This means the light falls off resonance quickly, seen as a sharp increase in the transmittance. When sweeping oppositely, the resonance shift is not as large as the former case. That is because, as the power starts to be coupled into the microring resonator, the thermo-optic effect red shifts the resonance, opposite to the sweeping direction, so that the off-to-on resonance and the following on-to-off resonance processes are too fast to record the zero-detuning point exactly. As seen in the spectrum, there is a sharp decrease in the transmittance, but the extinction ratio is much less than the former case. With the on-going sweeping toward shorter wavelength, the power coupled into the microring resonator decreases gradually, as the resonance returns back to

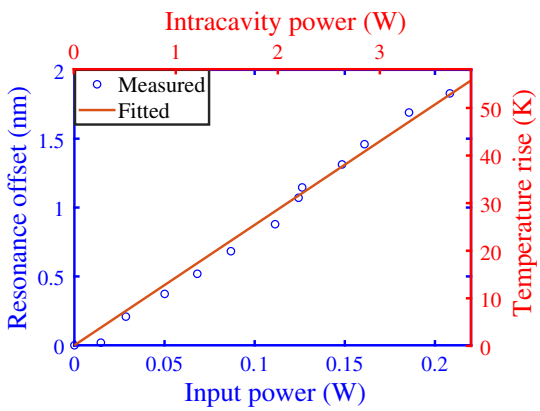

Figure 3. Measured (blue circles) and fitted (red line) resonance offset of the microring resonator with respect to the input power (left and bottom axis), corresponding to the relation between the local temperature rise and the intracavity power in the microring resonator (right and top axis).

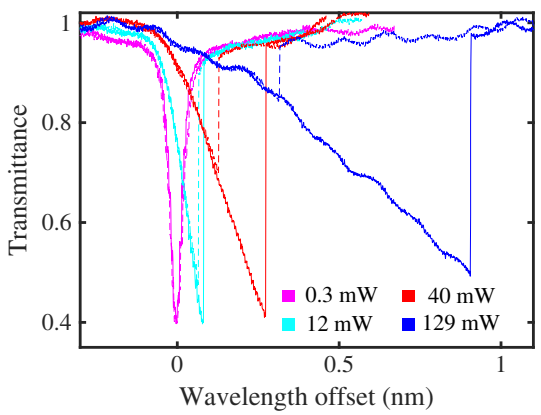

Figure 4. Optical bistability measured by sweeping the resonance from short to long wavelength (solid lines) and from long to short wavelength (dash lines) at different input powers.

Table 2. Thermal properties of 4H-SiC microring resonators acquired in this work.

Parameter	Value
$\frac{d\lambda}{dT}$	0.0344 nm K^{-1}
$\frac{dn_{eff}}{dT}$	4.21×10^{-5} K^{-1}
$\frac{df_{FSR}}{dT}$	−0.011 GHz K^{-1}
$\frac{dn_g}{dT}$	5.7×10^{-5} K^{-1}
$\frac{d\lambda}{dP_{input}}$	8.7 nm W^{-1}
$\frac{dT}{dP_{intra}} \left(\frac{\eta_{abs}}{\eta_{diff}}\right)$	14.9 K W^{-1}

original wavelength following the sweeping wavelength. The different routes in two sweeping directions and leaping transmittance make possible monolithic all-optical modulators, switching and read–write memory devices on the 4H-SiCOI integrated platforms.

In summary, the thermal effect related parameters that have been extracted from Section 2 are listed in **Table 2**.

3. Dual-Pump OPO

From the above-mentioned section, we know the relationship between the input power and the resonance red shift, and it is possible to reach on resonance by sweeping the light from short wavelength to long wavelength. The sweeping strategy can be applied to a practical experiment to generate OPO in a 4H-SiCOI microring resonator. The two adjacent fundamental TE resonances are at 1563.27 and 1567.22 nm, measured at low input power and room temperature. Two TE-polarized continuous-wave (CW) pumps are amplified by the erbium-doped fiber amplifier (EDFA). One pump, used for sweeping, has an on-chip power of 67 mW, which is high enough to induce a resonance red shift of 0.54 nm, according to Figure 3. Thus, it is swept from 1566.76 to 1567.76 nm. The other pump with an on-chip power of 45 mW is set at 1563.81 nm, which is one FSR apart from the stop wavelength of the sweeping pump. As two pumps start to resonant in the microring resonator, OPO is generated. However, with the second pump coupled into the microring resonator, the resonance is expected to be at longer wavelength. By monitoring the idler power, the wavelength of the two pumps can be moderately tuned to achieve the maximal output. As a result, the two pumps are able to be kept on resonances simultaneously and stably, without using the TEC for the external temperature controlling. Through the pump sweeping scheme to make both pumps on resonance, OPO is generated in the 4H-SiCOI microring resonator. As shown in **Figure 5**a, there are four new frequencies beside the two pumps, based on the cascaded FWM. The OPO spectrum is expected to be symmetric, as shown in Figure 5b, which is simulated based on the Lugiato–Lefever equation using the same conditions as in the experiment[45]

$$t_R \frac{\partial A}{\partial t} = \left[-(\alpha_t + i\delta_0) - i\frac{\beta_2 L}{2}\frac{\partial^2}{\partial \tau^2} + i\gamma L|A|^2]A + \sqrt{\kappa}[\sqrt{P_2} + \sqrt{P_1}\exp(i2\pi q f_{FSR}\tau - i2\pi\Delta t)\right] \tag{10}$$

Here, A is the optical field, t_R is the round-trip time, t is the slow time, α_t is the total loss including the propagation loss and the coupling loss, τ is the fast time, δ_0 is the relative detuning between Pump 2 and its nearest resonance, $\beta_2 = -115\,\mathrm{ps^2\,km^{-1}}$ is the simulated group velocity dispersion, $\gamma = \frac{n_2\omega}{cA_{eff}}$ is the nonlinear coefficient with the effective area of $A_{eff} = 0.43\,\mu\mathrm{m}^2$, P_1 and P_2 correspond to the on-chip power of Pump 1 and Pump 2, respectively, q is an integer describing that the resonance frequencies closed to the two pumps have an interval of qf_{FSR}, and Δ is the difference of the detuning between the two pumps, in the unit of Hz. Thus, we can predict there are two more new frequencies on the shorter wavelength side of the pump, but they are currently hidden beneath the high amplified spontaneous emission noise generated from the EDFA. The high propagation loss limits the efficiency of the OPO generation.

Based on the measured thermal properties, we also simulate the generation of Kerr soliton using the thermal tuning method. The separation of the two pump wavelengths is around one FSR, albeit with the detuning of Pump 1 slightly larger than that of Pump 2, so that the thermo-optic effect can be balanced.[46] Figure 5c shows that, if the propagation loss can be reduced to 2 dB $\mathrm{cm^{-1}}$, microcavity solitons with a spectral width exceeding 400 nm can be expected through linearly reducing the temperature by 20 K, with Pump 1 of 16 mW at 1562.60 nm and Pump 2 of 67 mW at 1566.57 nm. This result shows that, through the thermal tuning method, high-fidelity soliton frequency

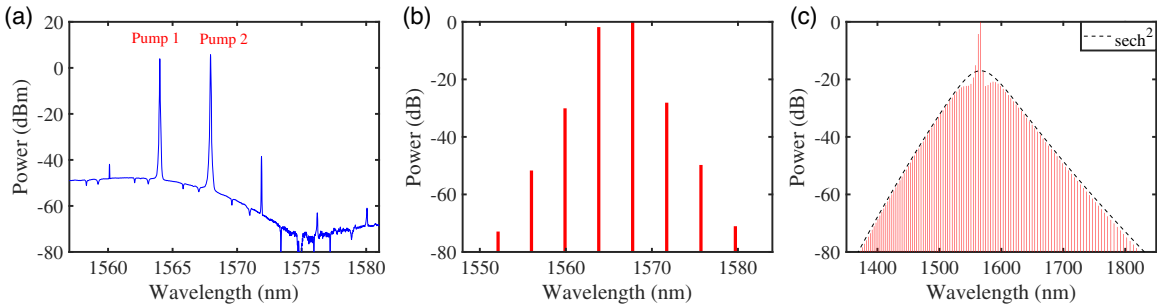

Figure 5. a) The measured spectrum of the TE polarized dual-pump OPO in a 4H-SiC microring resonator. The adjacent frequency lines are separated by one FSR. b) The simulated result of the TE polarized dual-pump OPO in a 4H-SiC microring resonator. c) The simulated result of soliton frequency comb generation through thermal tuning. A sech^2 fit shows the envelope of the soliton spectral shape.

combs can feasibly be generated experimentally in the 4H-SiC microring resonators with two fixed CW lasers. The frequency comb generation is currently limited by the low quality factor of the microring resonator, due to the large propagation loss. The loss is mainly contributed by the material absorption loss and the waveguide scattering loss, which could be improved by the high temperature annealing to recover the defects in the SiC thin film and by the chemical mechanical polishing of the 4H-SiCOI chip to reduce the surface roughness, respectively.

4. Conclusion

In this work, we characterize the thermal behaviors of a 4H-SiC microring resonator and study the thermal properties of the 4H-SiC waveguides with subwavelength dimensions. Either surrounding temperature variation or absorption-induced self-heating can exert thermal effects on the devices. On the other hand, the thermo-optic modulation and optical bistability of the 4H-SiC material make multifunctional optical-integrated devices possible. Furthermore, We experimentally demonstrate dual-pump OPO in the 4H-SiC microring resonator and numerically show that soliton frequency comb generation is achievable in the 4H-SiC integrated platforms through thermal tuning of the microring resonator. As the transmission window of SiC is quite wide, such a frequency comb has a considerable potential to extend the operation bandwidth to the visible and mid-IR wavelength range.

5. Experimental Section

4H-SiCOI Microring Resonator Fabrication: The 4H-SiCOI chip was fabricated through the ion-cut process.[47] The waveguide fabrication started from the 4H-SiCOI chip with 500 nm SiC top layer and 2.1 µm buried oxide layer. The positive resist AR-P 6200.09 was spun on the chip with a thickness of 210 nm. The pattern was defined by standard electron-beam lithography (JEOL JBX-9500FSZ) and was then transferred to a 70 nm aluminum hard mask, which was made by the electron-beam evaporation and a lift-off process. The sidewall of the hard mask was smoothed afterward by dipping the chip into the diluted phosphoric acid. The chip was etched by inductively coupled plasma reactive ion etching with SF_6, so that the pattern could be transferred onto the SiC layer. After striping the mask, the chip was wet oxidized to reduce the SiC thickness down to 400 nm and to smoothen the surface and the sidewall of the waveguides at the same time. Finally, 2.3 µm thick SiO_2 was deposited by plasma-enhanced chemical vapor deposition on top of the chip.

Experimental Setup: **Figure 6** shows the schematic of the experimental setup to measure the thermal behaviors. One CW laser, used for launching high power into the microring resonator, is amplified by an EDFA and then connects to a tunable attenuator and a polarization controller (PC) to control the input power and the polarization, respectively. The other laser, used for characterize the resonance at low power, is connected to a PC. Two paths of light are then combined with a 10 dB coupler and coupled in and out of the waveguide though a pair of grating couplers. The output light is split through another 10 dB coupler. One branch goes into an optical spectrum analyzer (OSA), to measure the spectral properties. The other branch, after connecting to an attenuator and a photodiode, goes into an oscilloscope (OSC), to measure the dynamic properties.

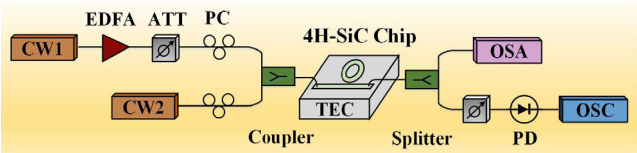

Figure 6. Experimental schematic of the thermal effect measurement. CW: continuous-wave laser, EDFA: erbium-doped fiber amplifier, ATT: tunable attenuator, PC: polarization controller, TEC: thermoelectric cooler, PD: photodiode, OSA: optical spectrum analyzer, and OSC: oscilloscope.

Acknowledgements

X.S. and W.F. contributed equally to this work. This work was supported by the European Union's Horizon 2020 FET Open (SiComb, No.899679).

Conflict of Interest

The authors declare no conflict of interest.

Data Availability Statement

The data that support the findings of this study are available from the corresponding author upon reasonable request.

Keywords

integrated photonics, microring resonators, nonlinear optics, silicon carbide, thermo-optic effects

Received: March 4, 2021
Revised: May 28, 2021
Published online: August 5, 2021

[1] J. Wang, F. Sciarrino, A. Laing, M. G. Thompson, *Nat. Photonics* **2020**, *14*, 273.
[2] R. Won, *Nat. Photonics* **2010**, *4*, 498.
[3] J. Leuthold, C. Koos, W. Freude, *Nat. Photonics* **2010**, *4*, 535.
[4] D. J. Moss, R. Morandotti, A. L. Gaeta, M. Lipson, *Nat. Photonics* **2013**, *7*, 597.
[5] H. Jung, H. X. Tang, *Nanophotonics* **2016**, *5*, 263.
[6] C. Wang, M. Zhang, M. Yu, R. Zhu, H. Hu, M. Loncar, *Nat. Commun.* **2019**, *10*, 1.
[7] D. M. Lukin, C. Dory, M. A. Guidry, K. Y. Yang, S. D. Mishra, R. Trivedi, M. Radulaski, S. Sun, D. Vercruysse, G. H. Ahn, J. Vučković *Nat. Photonics* **2020**, *14*, 330.
[8] C. Eddy, D. Gaskill, *Science* **2009**, *324*, 1398.
[9] K. Powell, A. Shams-Ansari, S. Desai, M. Austin, J. Deng, N. Sinclair, M. Lončar, X. Yi, *Opt. Express* **2020**, *28*, 4938.
[10] Y. Zheng, M. Pu, A. Yi, X. Ou, H. Ou, *Opt. Lett.* **2019**, *44*, 5784.
[11] F. Martini, A. Politi, *Appl. Phys. Lett.* **2018**, *112*, 251110.
[12] M. A. Guidry, K. Y. Yang, D. M. Lukin, A. Markosyan, J. Yang, M. M. Fejer, J. Vučković, *Optica* **2020**, *7*, 1139.
[13] X. Wu, T. Fan, A. A. Eftekhar, A. Adibi, *Opt. Lett.* **2019**, *44*, 4941.
[14] P. Xing, D. Ma, L. C. Kimerling, A. M. Agarwal, D. T. Tan, *APL Photonics* **2020**, *5*, 076110.
[15] B.-S. Song, T. Asano, S. Jeon, H. Kim, C. Chen, D. D. Kang, S. Noda, *Optica* **2019**, *6*, 991.
[16] S. Yamada, B.-S. Song, S. Jeon, J. Upham, Y. Tanaka, T. Asano, S. Noda, *Opt. Lett.* **2014**, *39*, 1768.
[17] D. O. Bracher, E. L. Hu, *Nano Lett.* **2015**, *15*, 6202.

[18] I. Chatzopoulos, F. Martini, R. Cernansky, A. Politi, *ACS Photonics* **2019**, *6*, 1826.
[19] M. Radulaski, T. M. Babinec, K. Müller, K. G. Lagoudakis, J. L. Zhang, S. Buckley, Y. A. Kelaita, K. Alassaad, G. Ferro, J. Vučković, *ACS Photonics* **2015**, *2*, 14.
[20] J. Y. Lee, X. Lu, Q. Lin, *Appl. Phys. Lett.* **2015**, *106*, 041106.
[21] X. Lu, J. Y. Lee, S. Rogers, Q. Lin, *Opt. Express* **2014**, *22*, 30826.
[22] S. Castelletto, B. C. Johnson, A. Boretti, *Adv. Opt. Mater.* **2013**, *1*, 609.
[23] X. Jiang, L. Yang, *Light: Sci. Appl.* **2020**, *9*, 1.
[24] P. Dong, R. Shafiiha, S. Liao, H. Liang, N.-N. Feng, D. Feng, G. Li, X. Zheng, A. V. Krishnamoorthy, M. Asghari, *Opt. Express* **2010**, *18*, 10941.
[25] P. Dong, W. Qian, H. Liang, R. Shafiiha, N.-N. Feng, D. Feng, X. Zheng, A. V. Krishnamoorthy, M. Asghari, *Opt. Express* **2010**, *18*, 9852.
[26] X. Xue, Y. Xuan, C. Wang, P.-H. Wang, Y. Liu, B. Niu, D. E. Leaird, M. Qi, A. M. Weiner, *Opt. Express* **2016**, *24*, 687.
[27] C. Joshi, J. K. Jang, K. Luke, X. Ji, S. A. Miller, A. Klenner, Y. Okawachi, M. Lipson, A. L. Gaeta, *Opt. Lett.* **2016**, *41*, 2565.
[28] M. Pöllinger, A. Rauschenbeutel, *Opt. Express* **2010**, *18*, 17764.
[29] K. Guo, L. Yang, X. Shi, X. Liu, Y. Cao, J. Zhang, X. Wang, J. Yang, H. Ou, Y. Zhao, *Phys. Rev. Appl.* **2019**, *11*, 034007.
[30] Z. Chai, X. Hu, F. Wang, X. Niu, J. Xie, Q. Gong, *Adv. Opt. Mater.* **2017**, *5*, 1600665.
[31] N. L. B. Sayson, T. Bi, V. Ng, H. Pham, L. S. Trainor, H. G. Schwefel, S. Coen, M. Erkintalo, S. G. Murdoch, *Nat. Photonics* **2019**, *13*, 701.
[32] T. Herr, K. Hartinger, J. Riemensberger, C. Wang, E. Gavartin, R. Holzwarth, M. Gorodetsky, T. Kippenberg, *Nat. Photonics* **2012**, *6*, 480.
[33] T. J. Kippenberg, S. M. Spillane, K. J. Vahala, *Phys. Rev. Lett.* **2004**, *93*, 083904.
[34] D. V. Strekalov, N. Yu, *Phys. Rev. A* **2009**, *79*, 041805.
[35] T. J. Kippenberg, A. L. Gaeta, M. Lipson, M. L. Gorodetsky, *Science* **2018**, *361*, 6402.
[36] H. Guo, M. Karpov, E. Lucas, A. Kordts, M. H. Pfeiffer, V. Brasch, G. Lihachev, V. E. Lobanov, M. L. Gorodetsky, T. J. Kippenberg, *Nat. Phys.* **2017**, *13*, 94.
[37] V. Brasch, M. Geiselmann, T. Herr, G. Lihachev, M. H. Pfeiffer, M. L. Gorodetsky, T. J. Kippenberg, *Science* **2016**, *351*, 357.
[38] B. Shen, L. Chang, J. Liu, H. Wang, Q.-F. Yang, C. Xiang, R. N. Wang, J. He, T. Liu, W. Xie, J. Guo, D. Kinghorn, L. Wu, Q.-X. Ji, T. J. Kippenberg, K. Vahala, J. E. Bowers, *Nature* **2020**, *582*, 365.
[39] K. Guo, X. Shi, X. Wang, J. Yang, Y. Ding, H. Ou, Y. Zhao, *Photonics Res.* **2018**, *6*, 587.
[40] A. Guarino, G. Poberaj, D. Rezzonico, R. Degl'Innocenti, P. Günter, *Nat. Photonics* **2007**, *1*, 407.
[41] T. Carmon, L. Yang, K. J. Vahala, *Opt. Express* **2004**, *12*, 4742.
[42] Z. Li, R. C. Bradt, *J. Appl. Phys.* **1986**, *60*, 612.
[43] S. Diallo, G. Lin, Y. K. Chembo, *Opt. Lett.* **2015**, *40*, 3834.
[44] P. Absil, J. Hryniewicz, B. Little, P. Cho, R. Wilson, L. Joneckis, P.-T. Ho, *Opt. Lett.* **2000**, *25*, 554.
[45] S. Zhang, J. M. Silver, T. Bi, P. Del'Haye, *Nat. Commun.* **2020**, *11*, 1.
[46] Z. Lu, W. Wang, W. Zhang, S. T. Chu, B. E. Little, M. Liu, L. Wang, C.-L. Zou, C.-H. Dong, B. Zhao, W. Zhao, *AIP Adv.* **2019**, *9*, 025314.
[47] A. Yi, Y. Zheng, H. Huang, J. Lin, Y. Yan, T. You, K. Huang, S. Zhang, C. Shen, M. Zhou, W. Huang, J. Zhang, S. Zhou, H. Ou, X. Ou, *Opt. Mater.* **2020**, *107* 109990.
[48] S. Yamada, B.-S. Song, T. Asano, S. Noda, *Opt. Lett.* **2011**, *36*, 3981.